

SUPPORTING INFORMATION

Enhanced Propylene Oxide Selectivity for Gas Phase Direct Propylene Epoxidation by Lattice Expansion of Silver Atoms on Nickel Nanoparticles

Bin Yu†, Tuğçe Ayvalı †, Elizabeth Raine, Tong Li, Molly Li, Jianwei Zheng, Simson Wu, Abdulaziz A. Bagabas and Shik Chi Edman Tsang

Content

Experimental Methods

Figure S1 TEM images of pure SBA-15

Figure S2 TEM image of a Ni core@Ag shell nanoparticle from $\text{Ni}_{0.4}\text{Ag}_1$ and $\text{Ni}_1\text{Ag}_{0.4}$ after SBA-15 template removal

Figure S3 Raw and fitted Ag and Ni K-edge EXAFS patterns for selected $\text{Ni}_1\text{Ag}_{0.4}/\text{SBA-15}$ catalyst in k and R spaces

Table S1 Ni K-edge EXAFS for Ni/SBA-15 and Ni@Ag/SBA-15 catalysts

References

Experimental Methods

Synthesis of SBA-15

The ordered silica-block copolymer mesoporous SBA-15 were synthesized by a modified method according to Zhao & Stucky's work.¹ In a standard preparation, 2 g of Pluronic P123 ($M_{av} = 5800$) was dissolved into 15 g of Milli-Q water and 60g of 2M HCl aqueous solution under stirring at 35-40 °C. 4.15 g of TEOS was then added into the homogeneous solution. The mixture was stirred at 35-40 °C for 20 h and crystallized at 100 °C for 2 days. The obtained solid product was then collected by filtering. The excess amount of P123 triblock copolymer was finally removed by calcination at 550 35-40 °C under air for 6 h to obtain Cal-SBA-15.

Synthesis of Ni@Ag/SBA-15 catalysts

The core@shell bimetallic Ni@Ag/SBA-15 catalysts with a silver loading of 5 wt% were prepared using a co-impregnation method according to our previous report.² In a typical preparation, known amounts of AgNO₃ and Ni(NO₃)₂·6H₂O were dissolved in Milli-Q water. SBA-15 was then added to the prepared solution under vigorous stirring at room temperature. Then, the mixtures were subjected to aging for 12 h in dark and dried in oven at 100 °C overnight. The obtained sample was calcined at 350 °C in N₂ for 4 h and further reduced in dilute H₂ for 3 h to produce the Ni@Ag/SBA-15 catalyst. Ni@Ag/SBA-15 catalysts with various Ni/Ag molar ratios, monometallic Ag/SBA-15 and Ni/SBA-15 were all prepared using the previously described method. The higher Ag content bimetallic catalysts were denoted as Ni_xAg₁/SBA-15, where x (0.2 and 0.4) represents the atomic ratio of Ni to Ag; and the low Ag content bimetallic catalysts were denoted as Ni₁Ag_y/SBA-15, where y (0.4 and 0.2) represents the atomic ratio of Ag to Ni. Similarly, monometallic Ag/SBA-15 and Ni/SBA-15 were also prepared for the comparison.

Catalytic testing

All the gas-solid phase reactions were performed in a vertical tubular fixed bed reactor which allowed three stages of temperature control throughout the whole reactor to deliver evenly distributed temperature. The gas flow was controlled and mixed by mass flow controller (Brooks SLA5850s) with an error range of ± 0.05 mL/min. The reactants and products were

analysed online by a gas chromatograph (Shimadzu GC-2014) equipped with a methanizer and a flame ionization detector (FID).

Temperature effect on Ni_{0.4}Ag₁/SBA-15 activity

In a standard reaction, 50 mg of Ni_{0.4}Ag₁/SBA-15 was packed in the middle stage of the reactor with quartz wool on the top and bottom of the catalysts. The composition of the feeding gas mixture was 5% C₃H₆ in helium and 5% O₂ in helium with a mix ratio of 2:1 (3.33% C₃H₆: 1.67% O₂ : 95% He) at a total flow rate of 20 mL/min, which was delivered from the top of the reactor and the reaction pressure was at 1 bar. A temperature program was used, beginning at 100 °C to 330°C, at each reaction temperature point (every 10 °C from 100-330 °C), the reaction was kept for 1 h allowing the GC to analyse the reaction products.

Effect of GHSV on catalytic activity

The Ni_{0.4}Ag₁/SBA-15 catalyst was tested under isothermal conditions at 220 °C with 5 different loadings, namely: 50 mg, 100mg, 200mg 300mg and 500mg while keeping the total gas flow the same. In a standard reaction, a known amount of Ni_{0.4}Ag₁/SBA-15 was packed in the middle stage of the reactor with quartz wool on the top and bottom of the catalysts. The composition of the feeding gas mixture was 5% C₃H₆ in helium and 5% O₂ in helium with a mix ratio of 2:1 (3.33% C₃H₆ : 1.67% O₂ : 95% He) at a total flow rate of 20 mL/min, which was delivered from the top of the reactor and the reaction pressure was at 1 bar. The isothermal reaction test was kept at 220 °C for 1 h allowing the GC to analyse the reaction products. The results were presented at gas hourly space velocity (GHSV) (h⁻¹) in the main text.

Here, we have investigated the temperature and GHSV effects of Ni_{0.4}Ag₁/SBA-15 catalyst on PO production based on the high conversion and selectivity observed in catalytic hydrogenation of dimethyl oxalate to methyl glycolate or ethylene glycol based on our previous study (Chem. Commun., 2016, 52, 2569–2572).

After the optimization of these two parameters, Ag/Ni ratio was then changed as shown below to study the effect of shell thickness.

Effect of Ni/Ag molar ratio on the catalytic performance

The catalysts performances, including Ag/SBA-15, Ni_{0.2}Ag₁/SBA-15, Ni_{0.4}Ag₁/SBA-15, Ni₁Ag_{0.4}/SBA-15 and Ni₁Ag_{0.2}/SBA-15, were tested under isothermal conditions at 220 °C. In a standard reaction, 500 mg of catalyst was packed in the middle stage of the reactor with

quartz wool on the top and bottom of the catalysts. The composition of the feeding gas mixture was 5% C₃H₆ in helium and 5% O₂ in helium with a mix ratio of 2:1 (3.33% C₃H₆ : 1.67% O₂ : 95% He) at a total flow rate of 20 mL/min, which was delivered from the top of the reactor and the reaction pressure was at 1 bar. The isothermal reaction test was kept at 220 °C for 1 h allowing the GC to analyse the reaction products.

Stability Test

Catalysts stability tests were conducted to evaluate the stability of Ag structure during the selective propylene oxidation reaction over Ag/SBA-15, Ni_{0.2}Ag₁/SBA-15, Ni_{0.4}Ag₁/SBA-15, Ni₁Ag_{0.4}/SBA-15 and Ni₁Ag_{0.2}/SBA-15. In a standard reaction, 500 mg of catalyst was packed in the middle stage of the reactor with quartz wool on the top and bottom of the catalysts. The composition of the feeding gas mixture was 5% C₃H₆ in helium and 5% O₂ in helium with a mix ratio of 2:1 (3.33% C₃H₆ : 1.67% O₂ : 95% He) at a total flow rate of 20 mL/min, which was delivered from the top of the reactor and the reaction pressure was at 1 bar. The stability test was kept at 220 °C for 10 h, and the reaction products were analysed by GC every hour.

Characterisation

Synchrotron Powder X-Ray Diffraction (SXRD)

SXRD measurements were conducted on Beamline I11, Diamond Light Source (Diamond, Harwell, UK) by Dr Ben Lo of our group member. The energy of the incident X-ray flux was set at 15 keV, the wavelength and the 2 θ -zero point were refined using a diffraction pattern obtained from a high-quality silicon powder (SRM640c), corresponding to $\lambda=0.826617(4)$ Å and $2\theta_{\text{ZP}} = -0.000254(10)^\circ$. High resolution SXRD data were obtained from the zeolite samples using the multi-analyser crystals (MAC) detectors. The patterns were collected in the 2 θ range 0-150° with 0.001° data binning.

Low and High Resolution Transmission Electron Microscopy (HR-TEM)

TEM was performed using the JEOL 2010 and JEOL 300 operating at 200 kV. Samples for TEM analysis were prepared by dispersing a small amount of material (typically 1 mg) in approximately 1 mL of ethanol. One drop of the dispersion was placed onto a copper grid (holey carbon supported on copper, 400 mesh) and the solvent evaporated in air prior to analysis. Average particles size distributions and the histogram were calculated from the measurement of at least 150 individual particles.

High Sensitivity Low-Energy Ion Scattering (HS-LEIS)

All the experiments were performed in a combined elevated-pressure reaction cell-ultrahigh vacuum (UHV) system by Dr Jianwei Zheng of Xiamen University, China. Both sample preparation and testing were conducted in the primary UHV chamber (base pressure, 2×10^{-9} Torr). HS-LEIS were measured by IONTOFQtac100 using $^{20}\text{Ne}^+$ (5 keV) as ion source. The scattering angle was 145° .

Atom Probe Tomography (APT)

To prepare the APT sample, a drop of diluted Ag@Ni/SBA-15 colloidal dispersions was first placed onto a Si wafer. A 150 nm thick protective Cr-layer was then coated on top of the samples in the Cressington sputter coater. Needle-shaped APT specimens were prepared by means of a site-specific lift-out procedure using a FEI Helios G4 CX Nanolab focused ion beam (FIB)/scanning electron microscope. The APT experiments were conducted on a CAMECA LEAP 5000XR instrument equipped with an ultraviolet laser with a spot size of 2 μm and a wavelength of 355 nm. The detection efficiency of this state-of-the-air microscope is $\sim 52\%$. Data was acquired in laser pulsing mode at a specimen temperature of 60 K, with a target evaporation rate of 5 ion per 1000 pulses, a pulsing rate of 120 kHz, laser pulse energy of 80 pJ. The APT data were reconstructed and analysed using the commercial IVAS 3.6.14TM software by Dr Tong Li of Ruhr-Universität Bochum Universitätsstr.

X-Ray Photoelectron Spectroscopy (XPS)

XPS analysis was performed on a VG Escalab XPS Spectrometer operating under ultra-high vacuum (1×10^{-9} torr) using aluminium $K\alpha$ radiation with an energy of 1486.3 eV. Samples were prepared by depositing a thin layer of finely ground powder onto a double-sided sticky carbon tab attached to each sample holder. Wide scan spectra were acquired from 1 to 1200 eV to identify elements present in the sample, and were compiled from 4 scans with 0.1 sec dwell time, a 1 eV step interval, and a pass energy of 50 eV. Spectra of specific regions were obtained for elements of interest and were compiled from 15 scans with a 0.4 sec dwell time, a 0.1 eV step interval, and a pass energy of 20 eV. Data was processed using CasaXPS peak fitting software and binding energies were referenced to the C 1s peak corrected to a value of 284.50 eV to eliminate charging effects in accordance with the method by Jansen and van Bakkum.³

Extended X-Ray Absorption Fine Structure (EXAFS)

EXAFS measurements at the Ag K-edge and Ni K-edge were conducted on B18 beamline at Diamond Light Source (Diamond, Harwell, UK) to obtain information about the local structure of the Ni@Ag catalysts by Ms Molly Meng-Jung Li of our group member. Diamond installation comprises a 3 GeV electron storage ring with typical currents of 200mA, and B18 is a bending magnet beamline which has been designed to deliver monochromatic X-ray in the energy range of 2 to 35 keV. A Si (311) double crystal monochromator was used for energy selection with a resolution of 1 eV. Prior to the measurement, the samples were reduced in 5% H₂- 95% N₂. The reduced monometallic Ag/SBA-15, Ni/SBA-15 samples and bimetallic Ni@Ag/SBA-15 samples were loaded in the capillary tubes with the diameter of 3 mm. X-ray absorption spectroscopy data were collected at ambient temperature in transmission mode for the Ag K-edge measurements, while fluorescence spectra were acquired for the Ni K-edge measurements. Several scans were collected for each sample to get satisfactory data. The EXAFS data analysis was calibrated with foils as a reference to avoid energy shifts of the samples. The amplitude parameter was obtained from EXAFS data analysis of the foil, which was used as a fixed input parameter in the data fitting to allow the refinement in the coordination number of the absorption element. In this work, the first shell data analyses under the assumption of single scattering were performed with the errors estimated by R-factor.

The first shell analysis has been performed, taking the systematic errors of coordination number and the inter distances between the absorbing atom and neighbouring atoms into consideration. To perform the EXAFS fitting at Ag and Ni K-edge, Ag and Ni metals with standard fcc structures were taken from National Chemical Database Service (NCDS) as the primary models to generate the scattering paths of Ag-Ag⁴ and Ni-Ni,⁵ respectively. The scattering paths were applied to calculate the average number of neighbouring atoms for absorbing Ag or Ni. The corresponding $k^3\chi$ intensity and $k^3\chi$ phase corrected Fourier transform fitting curves for the samples were also derived. The experimental data for all the samples were recorded and satisfactory R fitting were achieved.

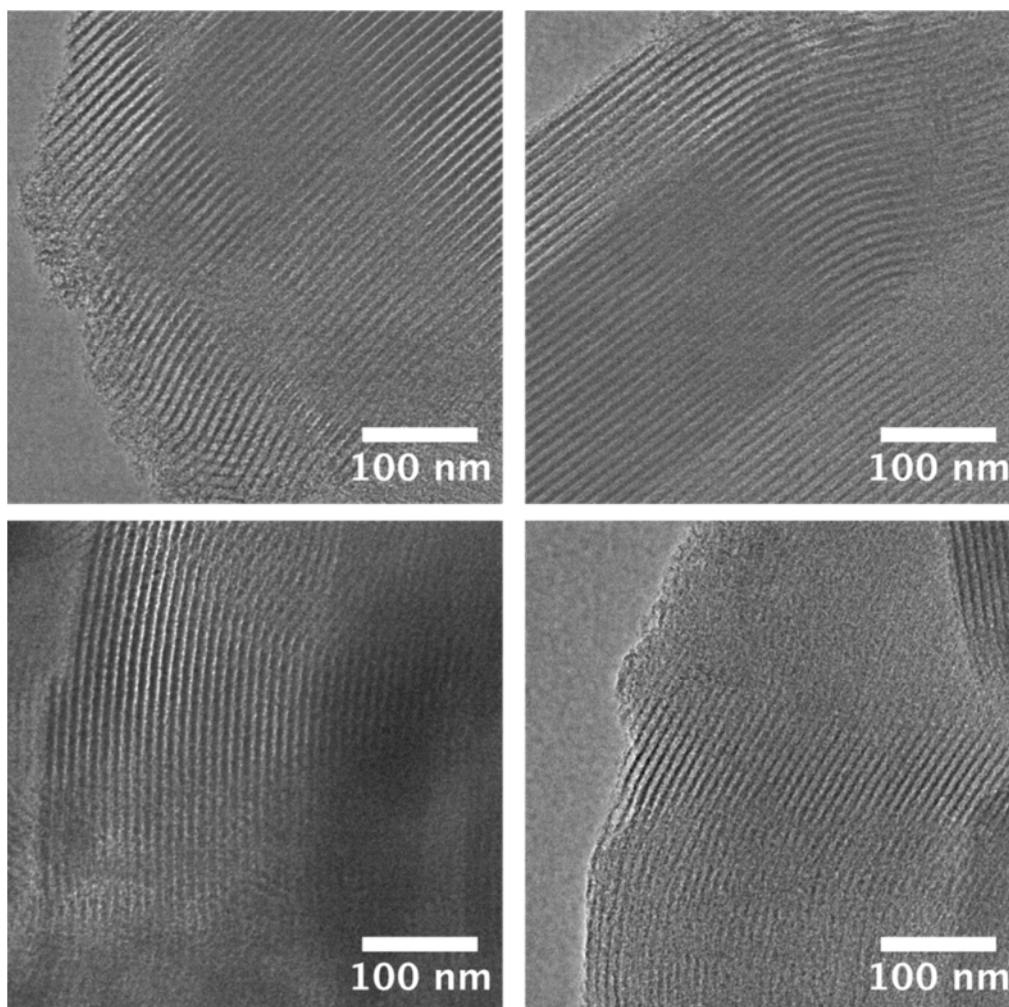


Figure S1 TEM images of pure SBA-15 showing the 4.6 ± 0.5 nm cylindrical porous channels alongside with the structure.

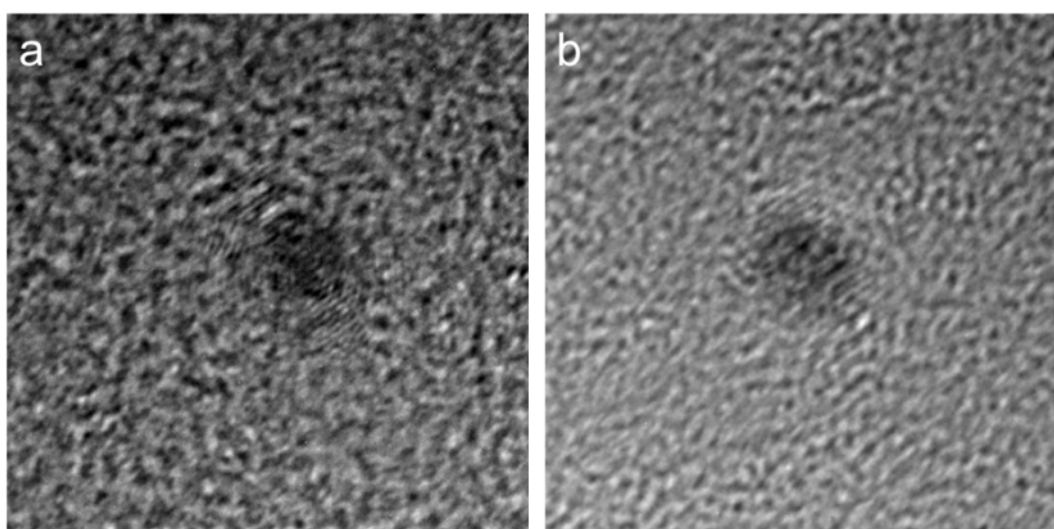


Figure S2 TEM image of a Ni core@Ag shell nanoparticle from a) $\text{Ni}_{0.4}\text{Ag}_1$ and b) $\text{Ni}_1\text{Ag}_{0.4}$ after SBA-15 template removal

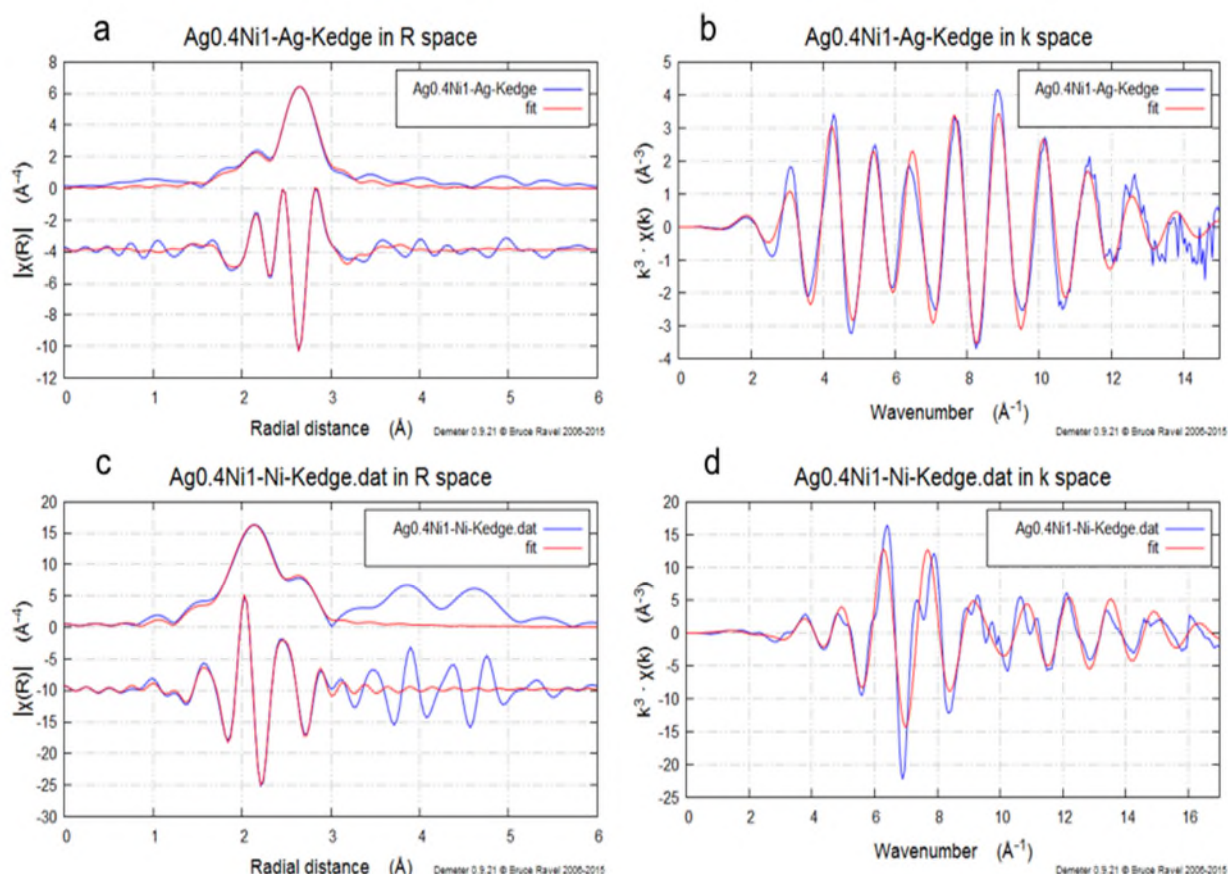


Figure S3 (a) Raw and fitted Ag K-edge EXAFS for selected Ni₁Ag_{0.4}/SBA-15; (b) Ag K-edge $k^3 \cdot \chi$ phase corrected Fourier transform of experimental and fitted data for Ni₁Ag_{0.4}/SBA-15; (c) Raw and fitted Ni K-edge EXAFS for Ni₁Ag_{0.4}/SBA-15; (d) Ni K-edge $k^3 \cdot \chi$ phase corrected Fourier transform of experimental and fitted data for Ni₁Ag_{0.4}/SBA-15

Table S1 Ni K-edge EXAFS for Ni/SBA-15 and Ni@Ag/SBA-15 catalysts; (Enot is difference in absorption energy between experiment and calculation)

Catalyst	Enot	CN (Ni-Ni)	D-W factor (Ni-Ni)	Bond length (Å) (Ni-Ni)	CN (Ni-Ag)	D-W factor (Ni-Ag)	Bond length (Å) (Ni-Ag)	R- factor
Ni _{0.2} Ag ₁ /SBA-15	-5.6	7.2(3)	0.005(1)	2.48(1)	4.2(6)	0.011(2)	2.78(1)	2.3%
Ni _{0.4} Ag ₁ /SBA-15	-4.8	7.7(3)	0.005(1)	2.48(1)	3.7(5)	0.010(1)	2.79(1)	1.5%
Ni ₁ Ag _{0.4} /SBA-15	-5.4	7.3(2)	0.005(1)	2.48(1)	3.0(3)	0.010(2)	2.79(2)	0.3%
Ni ₁ Ag _{0.2} /SBA-15	-5.5	7.6(2)	0.005(1)	2.48(1)	1.7(2)	0.011(2)	2.78(1)	0.4%
Ni/SBA-15	-5.1	8.0(4)	0.005(1)	2.48(1)	-	-	-	2.6%

Justification on the use of SBA-15 as a support

SBA-15 was chosen based on our previous study (*Chem. Commun.*, 2016, 52, 2569–2572). It has been shown that SBA-15 is a convenient template for the preparation of surfactant free and more well defined core-shell Ni-Ag catalysts. It is known that specific facets of Ag nanostructures are selective to propylene transformation to propylene oxide under oxygen and it is difficult to control the exposure of these specific facets in small size dimension. In this study, we aimed to engineer the thickness of Ag shell on Ni, thus the distance between Ag-Ag bond, in small scale by restricting the size of nanoparticles to the pore of SBA-15, *i.e.* 4.6 ± 0.5 nm, and study the reactivity of silver shell for direct propylene oxidation reaction using mesoporous SBA-15 as template. There is no strong support-metal interaction between the nanoparticles and template; therefore, SBA-15 was a right choice in order to study the reactivity of nanoparticles' surface.

Besides, many studies (please see the latest article concerning the subject: *ACS Catal.*, **2017**, 7 (4), pp 2668–2675) have shown that mesoporous high surface area supports are better for enhanced mass transfer of the molecules. However, propylene oxide may interact strongly with support groups leading to its decomposition. This is particularly pronounced if surface acidic groups on the support that could lead to isomerization or polymerization from the product mixture. Such surface interaction depends on the strength of surface acidity (low in case of silica based materials such as SBA-15), temperature and amount of adsorbate at the surface. The absence of chemisorption hysteresis in adsorption-desorption isotherm of propylene oxide on silica gel (E. Robinson and R. A. Ross, *J. Chem. Soc. A*, 1969, **0**, 2521–2525) indicates that there is no proton transfer from silica surface to propylene oxide thus the lack of ring opening and polymerization of propylene oxide.

Potential diffusion issues

There may have concerns on molecular diffusion to access active sites in zeolites. Rate limitation due to restricted diffusion is particularly pronounced due to blockage of 1-dimensional pores in liquid phase. It is however, the 3-D porous channels of SBA-15 are not easily blocked totally despite the fact it appeared to be plugged by several Ni@Ag nanoparticles. It would not hard for the particles to conform the 3-D pore networks. Gaseous substrate molecules (propylene, oxygen, propylene oxide and water) are still capable of diffusing between the interconnecting channels of SBA-15, as demonstrated in this paper. In addition, it has recently been shown that catalytic transformation of even larger molecules can be enhanced in the presence of embedded nanoparticles in the pores of SBA-15 (D. Bhuyan et. al. *Microporous and Mesoporous Materials* 256 (2018) 39–48).

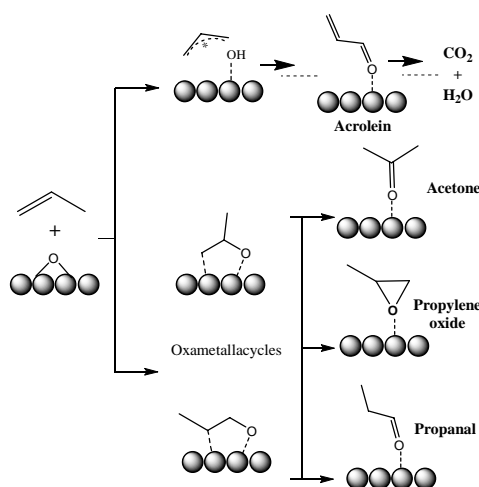
Surface acidity and basicity

It is generally known that acidity/basicity of the catalyst have important roles in selective propylene oxidation. Propylene oxide might interact with acidic groups of the support leading to isomerization or polymerization. But, as stated, such interaction depends on the strength of acid (low in case of silica based material such as SBA-15), temperature and amount of adsorbate at the surface. In addition, it has been shown that low basicity of oxygen atoms on Ag surface is the key for selective propylene epoxidation (D. Torres, N. Lopez, F. Illas, and R. M. Lambert, *Angew. Chem. Int. Ed.* 2007, 46, 2055–2058). Propylene epoxidation on

silver is strongly disfavoured by the markedly basic character of O_a , which leads to allylic hydrogen stripping and combustion. In order to reduce the basicity of oxygen adatoms, researchers use different techniques such as addition of alkali salt promoters, alloying, surface structure tailoring etc. Based on theoretical calculations (A. Pulido, P. Concepción, M. Boronat, A. Corma, *J. Catal.* 292 (2012) 138–147) and our unreported experimental results, the selectivity of propylene oxide over Ag(100) is much higher than Ag(111). This is attributed to the isolated active oxygen adsorbed on this facet with longer Ag-Ag interatomic distance for the effective epoxidation reaction. The neighbored oxyradical formed from dioxygen molecule on this facet does not catalyse the γ -H abstraction from the surface adsorbed oxygenated species in a favourable position to lead to the total combustion. Similarly, the synthesis of Ni@Ag core-shell nanoparticle and tailoring of Ag-Ag interatomic distance on Ag shell atoms may also provide a new way to create a longer Ag-Ag distance to reduce the total combustion route. Such longer interatomic Ag distance resulted from lesser surface packing can raise the surface d band centre to promote higher activity as according to the d band theory. Overall, due to the use of silica based SBA-15 and Ag catalyst, we believe that they will influence our study of the Ag lattice expansion by the Ni lattice.

Mechanistic aspects on propylene epoxidation

The mechanism of direct propylene oxidation with dioxygen over silver catalysts is well documented and accepted by many researchers. Please refer to: *ACS Catal.* 2014, 4, 32–39, *Angew. Chem. Int. Ed.* 2007, 46, 2055–2058; *J. Catal.*, 76, 333–344 (1982); *Chem. Phys. Lett.* 487 (2010) 183–189. Direct ethylene and propylene epoxidation over silver-based catalysts using oxygen as oxidizing agent are generally assumed to follow the same reaction pathway, which is schematically shown below. The mechanism starts with olefin adsorption on the oxidized silver surface, atomic oxygen being the active species. Activation of the allylic proton leads to formation of a radical intermediate that subsequently would generate acrolein and/or CO_2 , depending on the operating reaction conditions. Activation of the primary or secondary vinylic carbon atoms ends up with formation of a cyclic structure commonly referred as oxametallacycle (OMMP). From the OMMP complexes, carbonyl species are formed by transferring vinylic hydrogen, whereas by epoxidation, propylene oxide is obtained. The low selectivity of silver-based catalysts toward propylene epoxide has been related to the limited formation of the OMMP precursors, while the competitive allylic hydrogen abstraction is usually kinetically and thermodynamically more favourable.



References

- 1 D. Zhao, Q. Huo, J. Feng, B. F. Chmelka and G. D. Stucky, *J. Am. Chem. Soc.*, 1998, **120**, 6024–6036.
- 2 M. M.-J. Li, L. Ye, J. Zheng, H. Fang, A. Kroner, Y. Yuan and S. C. E. Tsang, *Chem. Commun.*, 2016, **52**, 2569–2572; J. Zhou et al. *Applied Catalysis A: General* 2015, 505 344–353.
- 3 R. J. J. Jansen and H. van Bekkum, *Carbon N. Y.*, 1995, **33**, 1021–1027.
- 4 D. E. Thomas, *J. Sci. Instrum.*, 1948, **25**, 440.
- 5 A. W. Hull, *Phys. Rev.*, 1917, **10**, 661–696.